

PROBE CORRECTED PLANE BI-POLAR NEAR-FIELD ANTENNA MEASUREMENTS

S.F. Gregson ^{*}, C.G. Parini [†], J. Dupuy [‡]

^{*}NSI, USA, sgregson@nearfield.com

[†]QMUL, UK, c.g.parini@elec.qmul.ac.uk

[‡]QMUL, UK, j.dupuy@elec.qmul.ac.uk

Keywords: Near-Field, Antenna Measurements, Plane Bi-Polar, Probe Pattern Correction.

Abstract

This paper introduces a simple transformation algorithm that enables probe-corrected, near-field and far-field data to be obtained from plane bi-polar near-field measurements [4, 9] which avoids the usual requirement to counter-rotate the probe and has the additional benefit of relaxing the restrictions that are usually placed upon the pattern of probe. Furthermore, this near-field to far-field transform, which avoids recourse to approximation [5, 2], is employed in combination with a minimum sampling scheme in order that measurement times can be reduced. Preliminary experimental results are presented and discussed.

1 Introduction

One of the principle problems associated with conventional planar near-field scanning is the cost and difficulty of producing one or more linear scanning axes. The plane polar method reduces this requirement to that of producing a single linear axis scanner but even this can be expensive to construct and can suffer from deviations from true linear. In an attempt to overcome this, and thereby further reduce cost, the plane bi-polar near-field scanning system has been proposed [9]. Here, the remaining linear scan axis is replaced with a second rotation axis operating much like the pickup arm of a record player. The dual parallel rotational axes, *i.e.* those of the antenna under test (AUT) and the probe arm, essentially enable the probe to sweep out an arc in two-dimensions thus enabling the collection of samples across the surface of a plane on a set of concentric rings. A corresponding simplification in the design of the guided-wave path is also obtained as only two rotary joints are required to connect the scanning probe to the stationary vector network analyser (VNA) thus insuring that phase stability is maintained across the entire scan plane. Furthermore, as the scan plane radius can be as great as twice the radius of the probe arm, this enables measurements to be taken across scan planes that are larger in physical extent than the measurement chamber [9, 8] although obviously the AUT still needs to fit within the chamber.

2 QMUL Plane Bi-Polar Near-Field System

The Queen Mary University of London (QMUL) plane bi-polar near-field antenna measurement system consisted of a vertical tower supporting an azimuth stage to which a counterbalanced horizontal beam was attached. This provided a support for a polariser and probe mounted on one end of the arm of the “record player” style scanner and which pointed vertically down. The resulting arc produced by the beam was set to the horizontal plane and set to an arbitrary but fixed length of approximately 1.2 meters. This measurement axis was used to sweep an arc across the path of the radiating AUT which was positioned below the probe pointing vertically upwards, *i.e.* anti-parallel with the probe, as illustrated schematically in Figure 1 whilst the sampling co-ordinate system can be seen in Figure 2. All metalwork was covered with appropriate absorber.

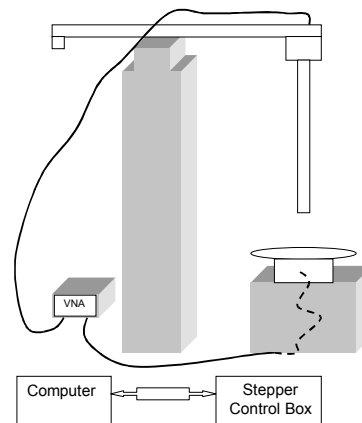


Figure 1: Plane bi-polar near-field antenna measurements system at QMUL.

The AUT was mounted on a second azimuth axis and mechanically aligned so that the rotational centres were co-centric and also in line with the centre of the probe, the “record player” arm being set at a convenient starting angle. Where rotations of greater than 45° were required, suitable rotary joints were put in place. For small angular movements phase stable cables were thought to suffice at frequencies below *circa* 20 GHz. The guided-wave RF connection to a VNA was made via flexible cables through a rotary joint on

the azimuth turntable to the AUT. On the probe side, a cable passed from the probe to a rotary joint then through a phase stable cable where the angle of arc changes on the scanning arm and finally back to the second port of the VNA.

As is usual for planar near-field measurements, the separation between the scanning probe and the AUT was such that the propagating portion of the radiated near-field was sampled. The length of the scanning arm was known and employed to calculate the sampling separation angle, which is also a function of the test frequency. Two initial scans were taken to find the peak signal strength and the location of a cross-polar null. Once this information was known, the scan parameters could be set and the signal levels within the system optimised. Samples were taken adhering to the Nyquist constraint of half a wavelength or smaller separation between adjacent samples. This was used to determine the number of samples taken on each of the concentric rings which increased as the radius of the ring increased. Scans were taken by incrementing the probe rotation stage and then scanning the AUT rotation stage. Stepper motors were used to drive all three of the axes. So, for a given ring an arm arc angle was chosen that matched exactly a given number of steps. Also, the azimuth rotation increment was chosen such that the number of steps for a given angle was exactly divisible into 360°. The number of concentric rings was determined by the sample increment and the required far-field pattern angle. This had the added benefit of enabling the first and last sample on a given ring to coincide. This redundancy could be used to compensate for any amplitude and phase drift within, what may potentially be, a comparatively long scan period. Two complete scans were taken. The first started with a co-polar alignment of the probe, *i.e.* its angular position derived from the cross-polar null, and the second with a “cross-polar” alignment, *i.e.* rotated through 90° from the previous case.

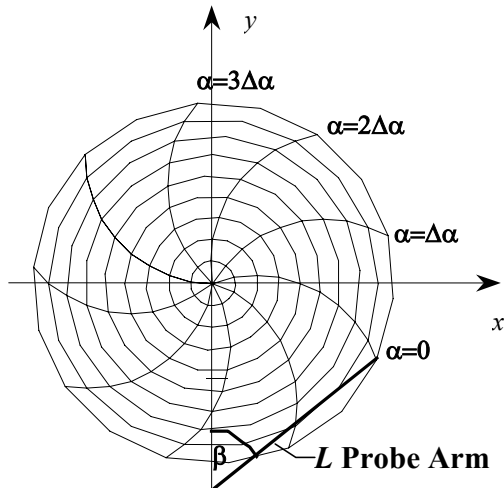


Figure 2: Plane bi-polar coordinate system.

3 Mathematical Basis

Two commonly encountered methods for accomplishing the necessary near-field to far-field transform of plane bi-polar measured data are:

- 1) Interpolate the data from a plane bi-polar measurement grid to a plane rectilinear grid and then utilise the standard plane rectilinear transformation techniques to obtain the far-field pattern.
- 2) Recast the near-field to far-field integral transform in terms of the plane-bi-polar co-ordinate systems and compute the far-field pattern directly from the measured samples.

The principal advantage of utilising interpolation is that the fast Fourier transform can be used to significantly improve the efficiency of the transform however, this is sought at the price of having to interpolate rapidly varying complex near-field data at a very early stage within the transformation processing chain. Conversely, deploying the near-field to far-field transform in each of these measurement geometries removes the requirement for such approximation but will inevitably increase the amount of computational effort required to obtain far-field data. However, the benefit of adopting this second approach is that, as will be shown below, it can be used to alleviate the need to counter-rotate the probe and can also be used to relax the restrictions that are commonly placed on the pattern of the probe when it is not counter-rotated.

The development of the general purpose near-field to far-field transform is presented in the following sub-sections which develop the plane bi-polar transform from the more commonly implemented plane-rectilinear method. The development is fairly general and with only very minor modification can be simplified to accommodate data acquired using a plane polar system.

3.1 Scalar Transform

It is widely known that the angular spectrum can be obtained directly from the sampled tangential near-field components using,

$$\underline{F}_T(k_x, k_y) = \int_{-\infty}^{\infty} \int_{-\infty}^{\infty} \underline{E}_T(x, y) e^{j(k_x x + k_y y)} dx dy \quad (1)$$

It is also known that, from an application of the stationary phase algorithm, the asymptotic far electric field can be very easily obtained from the angular spectrum since,

$$\underline{E}(k_x, k_y) \approx j \frac{e^{-jk_0 r}}{\lambda r} \frac{k_z}{k_0} \underline{F}(k_x, k_y) \quad (2)$$

Here, it is assumed that the normal field component is obtained from the tangential components using the plane wave condition, namely that $\underline{k} \cdot \underline{E} = 0$. Now, through the use of a multidimensional exchange of variables, it turns out to be a comparatively straightforward task to convert Equation (1) into a form that is directly applicable to the plane bi-polar measurements system where the samples are taken on a plaid, monotonic and equally spaced plane bi-polar grid. As in this case the transformation from Cartesian to plane bi-polar co-ordinates is a one-to-one mapping, and since $f(x, y)$ is

continuous and as the necessary partial derivatives exist and are also continuous, we may write that [1],

$$\iint_R f(x, y) dA_{x,y} = \iint_S f(x(u, v), y(u, v)) \left| \frac{\partial(x, y)}{\partial(u, v)} \right| dA_{u,v} \quad (3)$$

The transformation from plane bi-polar to Cartesian co-ordinates can be expressed as,

$$x = L(\sin(\beta - \alpha) + \sin \alpha) \quad (4)$$

$$y = L(\cos(\beta - \alpha) - \cos \alpha) \quad (5)$$

Here, the angles α and β denote the AUT rotation and probe arm angles respectively, L is the fixed length of the probe arm and the condition that $\beta \geq 0$ is observed. This, arrangement can be seen in Figure 2 above. Thus, once the necessary partial differentiation is performed and the resulting expressions have been simplified, the absolute value of the Jacobian can be written as,

$$\left| \frac{\partial(x, y)}{\partial(\alpha, \beta)} \right| = \left| \begin{array}{cc} \frac{\partial x}{\partial \alpha} & \frac{\partial x}{\partial \beta} \\ \frac{\partial y}{\partial \alpha} & \frac{\partial y}{\partial \beta} \end{array} \right| = \left| \frac{\partial x}{\partial \alpha} \cdot \frac{\partial y}{\partial \beta} - \frac{\partial x}{\partial \beta} \cdot \frac{\partial y}{\partial \alpha} \right| = L^2 \sin \beta \quad (6)$$

Thus, the Cartesian components of the angular spectrum of plane waves can be obtained directly from Cartesian electric field components sampled on a regular plane bi-polar grid using,

$$F(k_x, k_y) = L^2 \int_0^{\pi} \int_0^{2\pi} E(\alpha, \beta) e^{jL(k_x(\sin(\beta - \alpha) + \sin \alpha) + k_y(\cos(\beta - \alpha) - \cos \alpha))} \times \sin \beta d\alpha d\beta \quad (7)$$

3.2 Transformation of Polarisation Basis

Section 3.1 developed simple expressions that enable the angular spectrum, and therefore the corresponding far field pattern, to be obtained from samples that were tabulated on a plane bi-polar co-ordinate system. Within this section the question of the relationship between the unit vectors of the plane bi-polar and Cartesian co-ordinate systems is addressed. This can be quickly established using the usual formula [10],

$$\hat{e}_1 = \frac{\partial \mathbf{r}}{\partial u_1} \left/ \left| \frac{\partial \mathbf{r}}{\partial u_1} \right| \right. \quad (8)$$

Once the necessary differentiation has been performed the β directed unit vector can be expressed as,

$$\hat{e}_\beta = \cos(\alpha - \beta) \hat{e}_x + \sin(\alpha - \beta) \hat{e}_y \quad (9)$$

Taking the cross product of the z and β directed unit vector will determine the ‘‘effective’’ α orientated unit vector. Thus,

$$\hat{e}_\alpha = -\sin(\alpha - \beta) \hat{e}_x + \cos(\alpha - \beta) \hat{e}_y \quad (10)$$

The reason the approach of using a cross-product was taken is that the plane bi-polar co-ordinate system is not orthogonal at all points. That is to say, the α and β directed unit vectors are not mutually orthogonal for all values of α and β . However, when taking near-field antenna measurements we generally use a single probe and mechanically rotate it through 90°

about its axis between scans or alternatively, use an orthogonal mode transducer (OMT) to sample two orthogonal tangential near electric field components. When either of these procedures are adopted, the sampled field components are resolved onto the polarisation basis developed here, rather than onto a true plane bi-polar polarisation basis. This is shown schematically in Figure 3 below. By tracing the lines of increasing α and β it is apparent that, rather inconveniently and in contrast to the basis developed above, they are not mutually orthogonal. Here, the blue arrows represent the β orientated unit vectors whilst the black arrows represent the α orientated unit vectors.

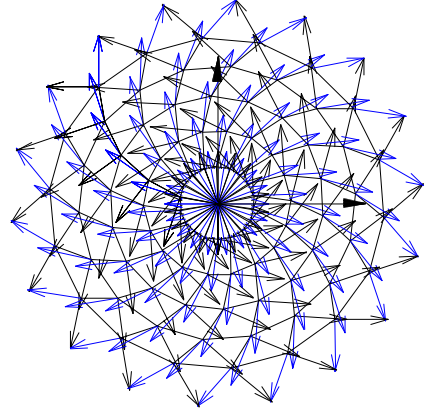


Figure 3: Illustration of measurement polarisation basis.

3.3 Rotated Probe Pattern Correction

The probe pattern can be thought of as a device that spatially filters the fields received from different parts of the AUT. It is not usually possible to neglect these effects in a planar range because of the large angles of validity required, and the short measurement distance employed. The necessary expressions required to correct the measured near-field data for the directive properties of the measuring probe can be shown to be [3, 6],

$$[A] = \frac{\lambda}{j} [M]^{-1} \cdot [P]^{-1} \cdot [S] e^{jk_z z_0} \quad (11)$$

Here, A is used to denote the probe corrected fields of the AUT, S are the angular spectra derived from the measured fields and $[M]^{-1}$ and $[P]^{-1}$ are,

$$[M]^{-1} = \frac{k_0}{k_z} \begin{bmatrix} (1 - k_x^2/k_0^2) & k_x k_y/k_0^2 \\ -k_x k_y/k_0^2 & -(1 - k_y^2/k_0^2) \end{bmatrix} \quad (12)$$

$$[P]^{-1} = \frac{1}{P_x^B(-k_x, k_y) P_x^C(-k_y, -k_x) + P_y^B(-k_x, k_y) P_y^C(-k_y, -k_x)} \times \begin{bmatrix} P_x^C(-k_y, -k_x) & P_y^B(-k_x, k_y) \\ P_y^C(-k_y, -k_x) & -P_x^B(-k_x, k_y) \end{bmatrix} \quad (13)$$

Here, the superscripts B and C are used to denote the angular spectra of the principally x -polarised and principally y -polarised measuring probes respectively, k_x , k_y and k_z are respectively the x , y , and z directed components of the propagation vector and k_0 is the free-space propagation

constant. In order that the probe pattern correction technique can be extended to accommodate the case where the probe has been rotated by an arbitrary fixed angle ϕ about the z -axis of the range all that is required is to rotate the pattern of the probe and the pattern of the, output, Hertzian dipole, and then to resolve the corrected fields back onto the range polarisation basis. The rotation of direction cosines is accomplished using the usual expressions namely,

$$\begin{bmatrix} k'_x \\ k'_y \end{bmatrix} = \begin{bmatrix} \cos \phi & \sin \phi \\ -\sin \phi & \cos \phi \end{bmatrix} \cdot \begin{bmatrix} k_x \\ k_y \end{bmatrix} \quad (14)$$

These rotated probe patterns, together with the rotated direction cosines are used in the probe pattern correction formula to obtain the probe pattern corrected field. The corrected field component can be resolved back onto the range polarisation basis using,

$$\begin{bmatrix} A'_x(k_x, k_y) \\ A'_y(k_x, k_y) \end{bmatrix} = \begin{bmatrix} \cos \phi & -\sin \phi \\ \sin \phi & \cos \phi \end{bmatrix} \cdot \begin{bmatrix} A_x(k_x, k_y) \\ A_y(k_x, k_y) \end{bmatrix} \quad (15)$$

In order that the validity of the probe pattern correction techniques discussed above could be thoroughly tested, a low gain AUT, in this case a standard gain horn (SGH), was acquired twice using a plane rectilinear near-field scanner. Once, with the AUT nominally aligned to the axes of the range and a second time with the AUT in the same orientation but with the scanning probe rotated around the range z -axis by 53° . A low gain instrument is preferable here, as the signal levels are relatively high at large angles so that errors in the correction are clearly observable. The probe-corrected far-field data can be found plotted in the form of contour, *i.e.* iso-level, plots in Figure 4 below. Here, the contours have been plotted in 5 dB steps from the peak of the pattern down. The measurements taken with the near-field probe nominally aligned with the axes of the range have been plotted using dotted contours whilst the unbroken lines are associated with measurements taken using a rotated probe. As can be seen, the agreement attained is encouraging with, although not shown here, similarly encouraging agreement attained for the case of the cross-polar pattern. Further information can be found in the literature [6, 7].

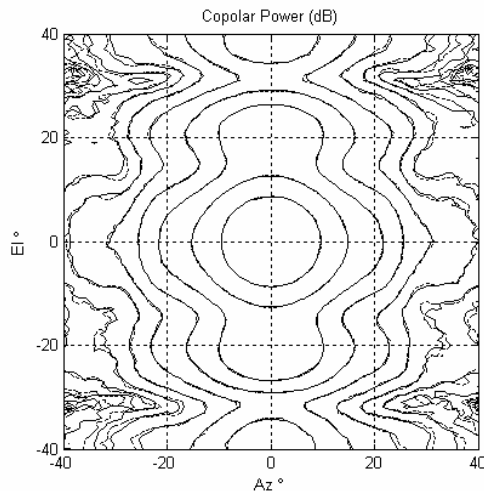


Figure 4: Comparison probe corrected far-field patterns taken using a nominally aligned and rotated near-field probe.

3.4 Near-Field to Far-Field Transform Algorithm

This section draws the results of the previous three sections together and describes how probe pattern corrected far-field data can be obtained from near-field measurements taken using a plane bi-polar measurement system.

The plane bi-polar measurement technique inherently rotates the probe about the range z -axis during an acquisition. Thus, the AUT-probe coupling will change differentially from sample to sample across the acquisition surface. This is not the case with plane rectilinear scanning where the angular relationship between the probe, the AUT, and the acquisition window is unchanged whilst characterising each of the near electric field components. If each set of rotated near-field data, *i.e.* in this case each individual point taken at a fixed rotation, ϕ , angle is transformed to the equivalent angular spectra, then the resulting pattern can be corrected using the generalised probe correction formula described above before being linearly superimposed on the all of the other corrected data sets. In this way, probe corrected far-field data can be obtained with no loss in rigour. The relationship between the angle through which the probe has been rotated and the bi-polar angles α and β can be obtained from geometry as,

$$\phi = \alpha - \beta/2 \quad (16)$$

As ϕ depends upon both α and β then essentially, the task of probe pattern correction formula and change in polarisation basis has been moved to the inside of the double integral of Equation (7). Although this approach still requires the use of approximation, *i.e.* interpolation, in the preparation of the probe pattern, the probe pattern is typically grossly over sampled, and by design will be a low gain, slowly varying far-field pattern function which is easily approximated.

4 Preliminary Results

Example near-field plane bi-polar measurements can be seen presented in Figure 5 and Figure 6 below. Here, although the orthogonal field components were sampled on a plane bi-polar grid, they have been displayed as though they had been tabulated on a regular Cartesian co-ordinate system. The near-field patterns have been plotted in this way purely to aid in the interpretation of the measured data sets. The samples were taken across an irregular plane bi-polar co-ordinate system so that the half wavelength sampling criteria is satisfied on each of the concentric rings thus maximising the efficiency of the measurement process, *i.e.* each concentric ring contains a different number of samples with the centre ring containing only a single sample for each polarisation. This can be accommodated within the transformation algorithm described above by simply modifying the elemental area associated with each sampled point. Here, an x -band corrugated horn was acquired using an open-ended rectangular waveguide (OEWG) probe.

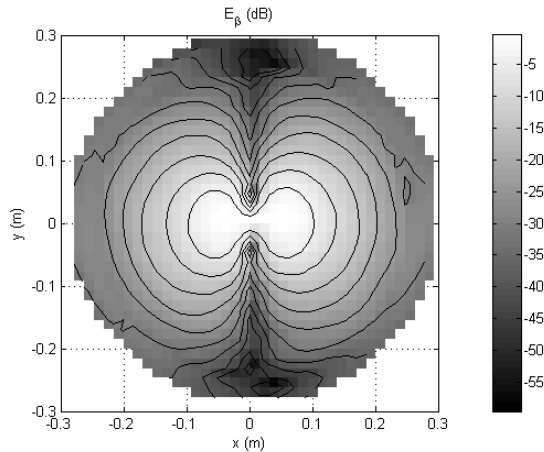


Figure 5: β -polarised near electric field component.

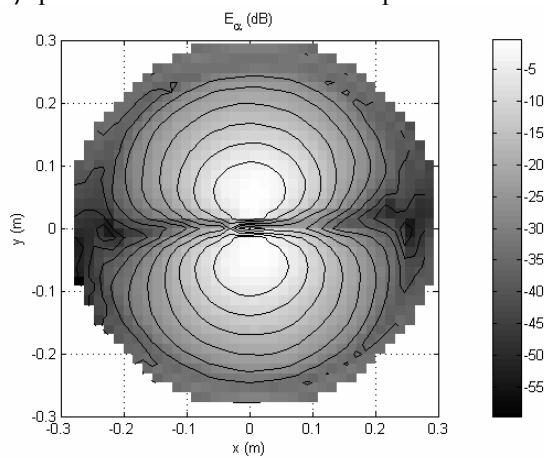


Figure 6: α -polarised near electric field component.

These data were transformed to the far field using the algorithm described above and the corresponding patterns can be found presented in Figure 7 and Figure 8 below. Here, the patterns have been tabulated on a regular azimuth over elevation co-ordinate system and the fields have been resolved onto a Ludwig III copolar and cross-polar polarisation basis. The size of the measurement plane and the separation between the AUT and the probe was such that the far-field pattern is valid only out to *circa* 40° from boresight.

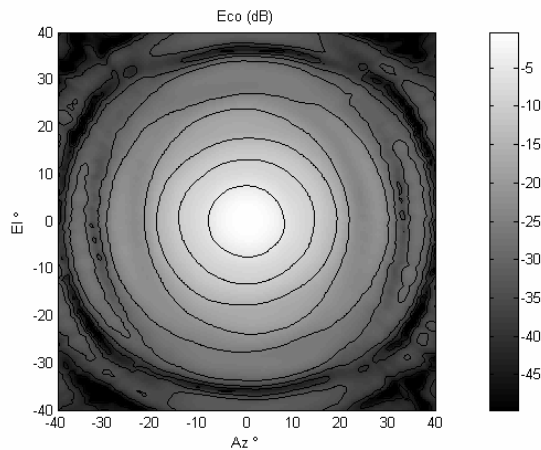


Figure 7: Copolar far-field pattern of x -band corrugated horn.

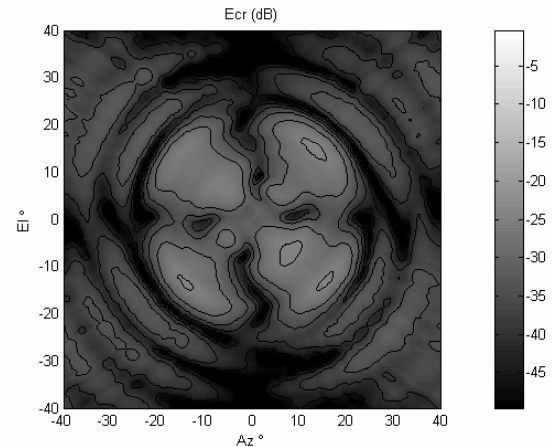


Figure 8: Cross-polar far-field pattern of x -band corrugated horn.

Figure 9 shows a comparison of the cardinal cuts obtained from the plane bi-polar measurement plotted together with a cardinal cut taken using a quasi far-field range.

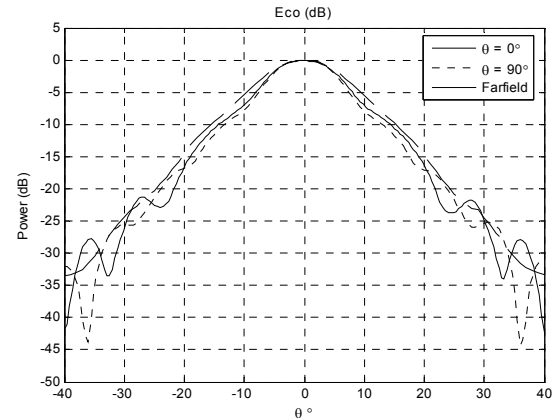


Figure 9: Comparison of horizontal and vertical cuts with direct far-field measurement.

The far-field patterns shown above are encouraging although some artefacts are present within these results that are very likely attributable to the measurement. From inspection of the cardinal cuts, it is evident that the agreement attained between the direct far-field and plane bi-polar measurements are not perfect. Here, the plane bi-polar results oscillate around the direct far-field measurement. Due to mechanical limitations within the experimental near-field system, the plane bi-polar measurement required an extended period of time to perform the measurements. Unfortunately, during this time the temperature and therefore the amplitude and especially the phase of the system was unfortunately able to drift. Fortunately, this could be seen within the near-field data itself and efforts to quantify and subsequently compensate for this drift are ongoing. This also resulted in introducing some channel imbalance between the sampled E_α and E_β field components. As the final far-field copolar and cross-polar patterns are formed from a combination of the sampled E_α and E_β field components any imbalance between these measured hands of polarisation will impact significantly

upon the quality and reliability of the ensuing far-field patterns and will be particularly evident within the cross-polar pattern function. In this case, this can be seen to manifest itself as an oscillatory ripple on the far field patterns and a slight raising of the level of the cross-polar pattern, i.e. a degradation in the cross-polar discrimination (XPD). However, it is a testimony to the inherent robustness of this technique that the accordance attained was achieved.

5 Summary and Conclusion

Within this paper the new QMUL plane bi-polar near-field measurement system has been presented. Encouraging results have been attained using this system in combination with a novel transformation algorithm. This system is still in its infancy and requires further work to improve the stability of the RF subsystem, to refine the robotic subsystem to increase the accuracy, precision and speed with which measurements can be taken in order that acquisition times can be further minimised. The principal benefits of this approach are:

- The construction of a simple three axes positioner system.
- The efficient use of sampling for a complex data pattern.
- Large antennas can be measured in a relatively small space.
- The new transformation algorithm relaxes previous restrictions on the types of near-field probes that can be used with plane polar, and plane bi-polar near-field measurement geometries.

Acknowledgements

The authors wish to express their gratitude to Miss Wendy West, Mr Bee Ho Goa and Mr Mahesh Patel for their contributions towards the experimental portion of the work.

References

- [1] H. Anton, "Calculus with Analytic Geometry", John Wiley & Sons, Inc., pp. 910, (1995).
- [2] O.M. Bucci, C. Gennarelli, C. Savarese, "Fast and Accurate Near-Field to Far-Field Transformation by Sampling Interpolation of Plane Polar Measurements", IEEE Transactions on Antennas and Propagation, AP-39, January, pp. 48-55, (1991).
- [3] R.H. Clarke & J. Brown, "Diffraction Theory and Antennas", Ellis Horwood Ltd., (1980).
- [4] V. Galindo-Israel, Y. Rahmat-Samii, R. Mittra, "A Plane-Polar Approach For Far-Field Reconstruction From Near-Field Measurements", Int. IEEE / AP-S Symp., Seattle, June, (1979).
- [5] M.S. Gatti, Y. Rahmat-Samii, "FFT Applications to Plane-Polar Near-Field Antenna Measurements", IEEE Transactions on Antennas and Propagation, AP-36, June, pp. 781-791, (1988).
- [6] S.F. Gregson, "Probe-Corrected Poly Planar Near-field Antenna Measurements", Ph.D. Thesis, University of London, (2003).
- [7] S.F. Gregson, A.J. Robinson, "An Inter-range Comparison in Support of the Characterisation of Space Antenna Systems and Payload Testing", IEE Colloquium on Antenna Measurements, 17th June, (1998).
- [8] J. McCormick, "The Use of Secondary Spatial Transforms in Near-Field Antenna Measurements", Ph.D. Thesis, Open University, (1999).
- [9] Y. Rahmat-Samii, L.I. Williams, R.G. Yaccarino, "The UCLA Bi-Polar-Near-Field Antenna-Measurement and Diagnostics Range", IEEE Antennas and Propagation Magazine, Vol. 37, No. 6, December, pp. 16-35, (1995).
- [10] M.R. Spiegel, "Theory and Problems of Vector Analysis and an Introduction to Tensor Analysis", Schaum Publishing Company, pp. 135, (1959).